James Raja *et al.*
*Beni-Suef Univ J Basic Appl Sci (2022) 11:103*
https://doi.org/10.1186/s43088-022-00281-5

Beni-Suef University Journal of Basic and Applied Sciences

RESEARCH Open Access

# Design of hexagonal chalcogenide photonic crystal fiber with ultra-flattened dispersion in mid-infrared wavelength spectrum

S James Raja[1*], Tony Jose[2], R Charlcedony[2], M Sam Paul[2] and R Chakravarthi[2]

**Abstract**

In the last few decades, silica-based photonic crystal fibers (PCFs) have been the subject of extensive research. Traditional silica-based PCFs, however, experience considerable propagation loss when used beyond 3000 nm. On the other hand, soft glasses, notably tellurite, fluoride, and chalcogenide glasses, offer exceptional optical transparency in the mid-IR wavelength region and are a desirable replacement for silica in MIR applications. A comprehensive investigation of chromatic dispersion properties in the hexagonal chalcogenide photonic crystal fibers is presented. The dependency of fiber dispersion on the structural parameters of photonic crystal fibers is thoroughly described in this study. Utilizing the interaction between material and geometrical dispersion, we were able to develop a well-defined framework for making specific predefined dispersion curves. In the mid-infrared wavelength spectrum, we are concerned with flattened, if not ultra-flattened, dispersion behaviors. In the wavelength range of 3500–6500 nm, the hexagonal chalcogenide microstructured fiber was engineered to achieve a typical dispersion profile flattened to within −3.41 to 9.5 ps/[nm–km] for the six-ring structure and −3.91 to 8.17 ps/[nm–km] for the four-ring structure. This proposed chalcogenide PCF can be used for soliton generation, gas sensing, biomedical imaging, supercontinuum generation, and long-distance high-speed communication applications in the mid-infrared wavelength range due to its nearly zero ultra-flattened dispersion characteristics.

**Keywords:** Nonlinear optics, Mid-IR supercontinuum generation, Chalcogenide glass, Infrared fibers, Microstructured optical fibers, Chalcogenide photonic crystal fiber, Dispersion-flattened, Chromatic dispersion, Ultra-flattened dispersion

## 1 Background

The unique kind of optical fibers known as photonic crystal fibers (PCFs) has a periodic arrangement of microcapillaries that forms the cladding of the fiber around a solid or a defective hollow core. The term "photonic crystal fiber" is derived from the distinctive cladding structure of this fiber type, in which the index differences are achieved by assembling a matrix of several materials with high and low refractive index. By doing this, a hybrid material is produced that has unique features that are not found in solid materials and an extent of index control that is not possible using conventional fibers. When compared to typical optical fibers, the PCFs' inherent versatility of design makes for a whole new range of novel characteristics, such as indefinitely single-mode transmission, extraordinarily high nonlinearity, high birefringence, and controllable dispersion. PCFs are commonly used in various fields such as optical communication and sensing because of these properties [1, 2].

In the last decade, some of the most advanced research and development have been carried out in the field of photonic crystals and their applications. Some of the notable developments are as follows: In [3], an effort

*Correspondence: james_p190157ec@nitc.ac.in

[1] Department of Electronics and Communication Engineering, National Institute of Technology Calicut, Calicut, India
Full list of author information is available at the end of the article

has been made to enhance the photonic bandgap width in a photonic crystal (PC) structure formed of a superconductor and a dielectric. A ternary photonic crystal has been used in photovoltaic applications as an optical broadband angular reflector in [4]. A 1D gyroidal PC structure has been designed for heavy metal concentration detection in fresh water in [5]. The tunability of transmission spectrum of a one-dimensional silica-based photonic quasicrystal has been studied in terahertz frequency range in [6]. In [7], a 1D ternary annular porous silicon PC has been designed for detection of chemical and biofluids. In [8] and [9], a PC-based optoelectronic device has been designed which can act as a temperature sensor with very high sensitivity. In [10], a wheel cladding with hexa-sectored core PCF has been designed for biodiesel fuel detection and monitoring. In [11] a 1D PC has been designed with a nanocomposite layer to be used for optical filtering applications in mode-locked lasers, solar cells, and optical switches.

In the last few years, there has been a lot of research into PCFs based supercontinuum (SC) laser sources that operate in the mid-infrared wavelength region. The widening of the spectrum caused by sufficiently powerful incident pulses propagating through a nonlinear medium is known as supercontinuum generation. Fiber-based supercontinuum (SC) laser sources covering the mid-infrared (MIR) are of enormous attraction for unveiling the knowledge and facts about the chemical structure of the element and material as well [12]. Most of the molecules experience vibrational absorption in the MIR wavelength range and therefore the MIR SC laser sources can be used for MIR spectroscopy to trace out the concentration of a molecular species of interest in the atmosphere [13]. The MIR SC sources have countless applications in several fields such as gas sensing [14], medical diagnostics [15], spectroscopy [16], and hyperspectral microscopy [17]. The atmosphere is transparent to the two spectral windows 3–5 $\mu$m and 8–13 $\mu$m and both the spectral windows lie in the MIR wavelength range. This will enable the SC sources to be used by industries as sensors to detect the poisonous and harmful gases in the atmosphere [18].

The main ingredients of glass are silicon and oxygen. Such glasses are oxide-based glasses. Silica-based PCFs have been widely researched in the past few decades. When used above 3 $\mu$m, however, traditional silica-based PCFs suffer from significant propagation loss [19]. As a result, using silica fiber for nonlinear applications in MIR, such as supercontinuum generation, is challenging. Soft glasses, such as tellurite (e.g., Te $O_2$), fluoride (e.g., Zr $F_4$ and Al $F_3$), and chalcogenide (e.g., S, Se, and Te) glasses, on the other hand, have outstanding optical transparency in the wavelength ranges of 0.5–5 $\mu$m, 0.4–6 $\mu$m, and 1–16 $\mu$m, respectively, and are therefore an appealing choice to replace silica in MIR applications [20, 21]. It is seen in Fig. 1 that ChGs exhibit a significantly larger infrared transparency window than oxide-based glasses. ChGs's IR transparency leads to a wide range of optical applications, as seen in Fig. 2.

Also, MIR SC sources based on soft glasses, notably chalcogenide, are required to perform applications in the MIR atmospheric windows due to their large nonlinear indices that may approach three orders of magnitude higher than silica. ZBLAN is the most robust fluoride glass material for optical fiber applications, but its nonlinear refractive index is comparatively low [24].

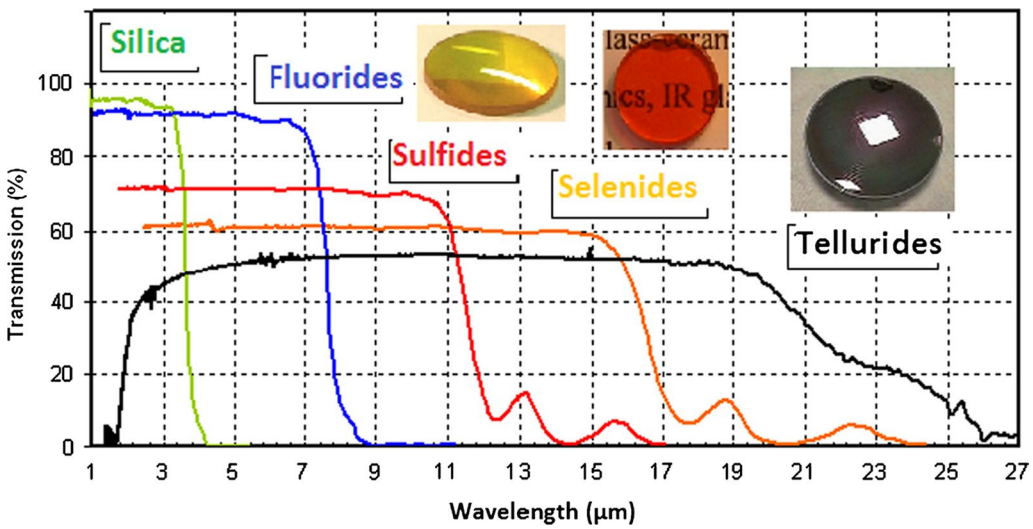


**Fig. 1** The optical transmission of ChGs in comparison to silica and fluoride glasses [22]

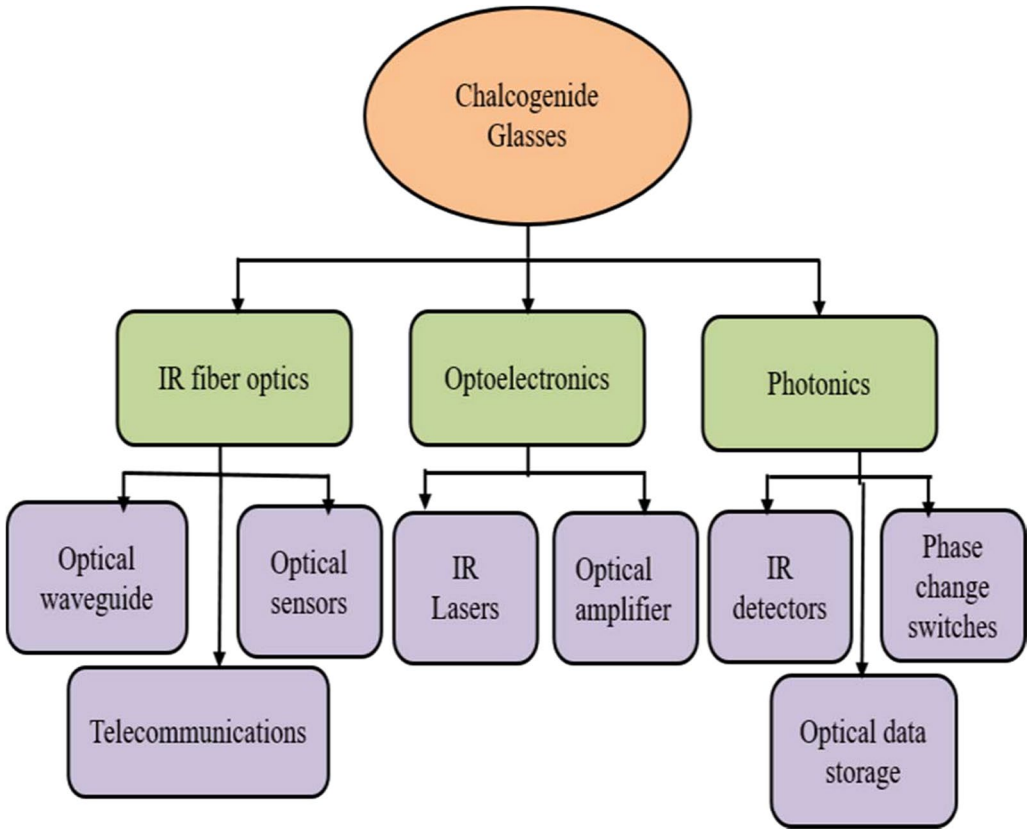


**Fig. 2** Different fields where ChGs are used [23]

Chalcogenide glass has a high nonlinear refractive index of $100 - 1000 \times 10^{-20} m^2 W^{-1}$ and an outstanding IR transmission up to 16 $\mu$m. However, it should be noted that the high nonlinearity and a good IR transmission alone does not guarantee MIR supercontinuum generation; a flattened dispersion profile is also essential. [25, 26].

We recall that an eleven ring PCF based on a circular structure was proposed by Reeves et al. This fiber achieved an ultra-flat dispersion with a dispersion variation of −0.6 to 0.6 ps/[nm–km] in the wavelength range of 1.24–1.44 $\mu$m [26]. Borhan et al. proposed a nine-ring PCF with a heptagonal configuration. In the wavelength range of 1.46–1.66 $\mu$m, this fiber obtained ultra-flat dispersion with a dispersion variation of −420.1 to −1160 ps/[nm–km] [27]. A three-ring PCF based on a hexagonal structure was proposed by Kokou et al. This fiber achieved a flattened zero dispersion from the visible region to the far infrared region [28]. Animesh et al. presented a nine-ring PCF with a circular topology. In the wavelength range of 1.35–1.70 $\mu$m, this fiber exhibited ultra-flat dispersion with a dispersion variation of −0.1252 to 0.1252 ps/[nm–km] [29]. A PCF based on a triangular structure was proposed by Albert et al. This fiber achieved an ultra-flat dispersion in the Ti–Za laser wavelength range (0.8 $\mu$m) and in the telecommunication window (1.55 $\mu$m) [30]. Anwar et al. presented a five-ring PCF with an octagonal construction. This fiber obtained an ultra-flat dispersion in the communications window (1.55 $\mu$m) [31]. A seven ring PCF based on a hexagonal structure was proposed by Mariusz et al. In the wavelength range of 1.1–2.7 $\mu$m, this fiber obtained ultra-flat dispersion with a dispersion variation of −50 to −30 ps/[nm-km] [32]. A slotted spiral PCF was proposed by Jianfei et al. This fiber achieved an ultra-flattened dispersion of 0.91 and 1.33 ps/[nm–km] over the wavelength range of 1.55 $\mu$m [33]. Takashi et al. suggested an eight-ring PCF with a hexagonal configuration. Over the telecommunication wavelength range, this fiber obtained an ultralow dispersion of less than 0.8 ps/[nm-km] [34]. In [35], a five-ring perforated core PCF has been designed with a large negative dispersion and a very high nonlinear coefficient for supercontinuum generation, dispersion compensation and high-speed data transmission applications. In [36], a rectangular slotted PCF core doped with GaP has been designed to yield a very high birefringence

and nonlinearity to be used in applications such as four-wave mixing, soliton generation, sensing, and biomedical imaging. In [37], a highly birefringent PCF with diamond-shaped porous core, hexagonal porous cladding with Zeonex background material has been proposed as polarization maintaining fiber for biomedical and long-distance high-speed communication applications. In [38] an ultra-high birefringent decahedron photonic crystal fiber with a large nonlinear coefficient has been designed for high-speed data transmission, dispersion compensation, soliton generation, and supercontinuum generation applications.

Looking through all of this literature, we noticed that the majority of highly birefringent, polarization maintaining dispersion-flattened fiber designs were focused on the telecommunication wavelength band. The mid-infrared (MIR) wavelength has recently piqued researchers' interest. This is due to the fact that the two primary atmospheric transmission windows are centered in this spectral region, and the light source in this region is considered as a strong tool for atmospheric surveillance, explosives tracking, and free-space communication [13]. The MIR is also regarded as the "fingerprint" area, where several molecules' vibration modes are found. This property makes MIR an important regime for biomedical applications [39, 40]. Therefore, in the recent years, PCF researchers have switched to chalcogenide glass which is a suitable alternative for silica material.

In this paper, we present a hexagonal chalcogenide PCF with broadband ultra-flattened dispersion in MIR. Glass materials comprising chalcogen elements from group 16 of the periodic table, such as sulfur (S), selenium (Se), and tellurium (Te), mixed with network-forming elements, such as silicon (Si), arsenic (As), germanium (Ge), phosphorous (P), and antimony (Sb) produces Chalcogenide glasses (ChGs). The dispersion properties of the PCF are studied and configured in detail as a function of fiber structure parameters. As a result, we demonstrate that the proposed fiber has a great deal of potential for MIR supercontinuum generation.

## 2 Methods

Figure 3 depicts a cross-sectional image of the proposed $Ge_{23}Sb_{12}S_{65}$ based chalcogenide PCF. The construction of the majority of photonic crystal fiber is geometrical. The array of holes is mostly tetrahedral, hexagonal, octagonal, quadrilateral, as well as many other shapes. PCF dispersion engineering may be done in a variety of ways [41]. On the other hand, the majority of the ways that have been proposed earlier in the literature are based on modifying the air-hole spacing (pitch) [42], air-hole diameter [43, 44], number of rings, and air-hole arrangement in circular, square, and

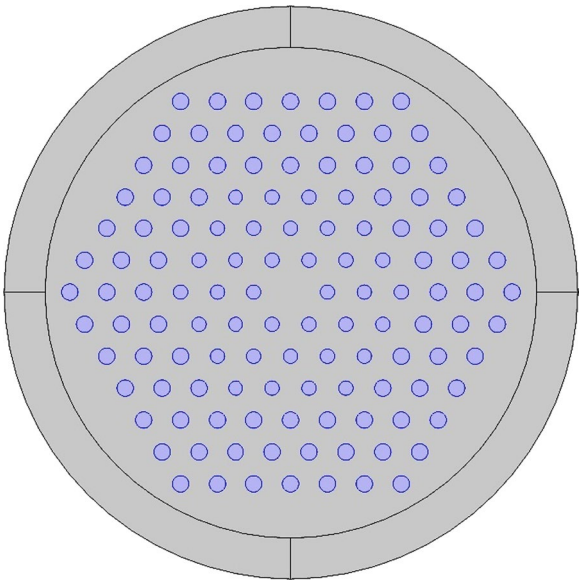

**Fig. 3** Cross-sectional image of the proposed $Ge_{23}Sb_{12}S_{65}$ based chalcogenide PCF

hexagonal lattices [45]. In our structure, the cladding is made up of six layers of air holes that are spaced out in a regular hexagonal pattern. We went for a hexagonal geometry since it would assist us in getting a better dispersion control and a very high birefringence. The air-hole spacing (pitch) was purposefully varied, allowing greater flexibility in dispersion engineering. The air holes in layers 1–3 have a diameter of 1.4 $\mu m$ and the air holes in layers 4–6 have a diameter of 1.6 $\mu m$. The hole spacing (pitch), $\Lambda$ of the optimized PCF is 5 $\mu m$. To prevent scattering losses from boundaries, a perfectly matched layer (PML) is deployed as an outer layer. The trinomial of the Sellmeier equation about lambda can be used to calculate the material dispersion of the $Ge_{23}Sb_{12}S_{65}$ glass.

$$n^2_{\mathrm{mat}}(\lambda) = A + \frac{B_1\lambda^2}{\lambda^2 - C_1} + \frac{B_2\lambda^2}{\lambda^2 - C_2} + \frac{B_3\lambda^2}{\lambda^2 - C_3} \quad (1)$$

where $\lambda$ is the wavelength in micrometers, and $C_1, C_2, C_3, B_1, B_2, B_3, andA$ are fitting coefficients of $Ge_{23}Sb_{12}S_{65}$ glass (Table 1).

Using COMSOL software that is based on the finite element method (FEM), the modal analysis is carried out numerically. The dispersion profile is flattened to within −3.41 to 9.5 ps/[nm–km] for the six-ring structure and −3.91 to 8.17 ps/[nm–km] for the four-ring structure for the optimum geometrical parameters in the wavelength range of 3500–6500 nm. At 3.3 μm, we determined that the most effective candidate for successful SC production

**Table 1** Fitting coefficients of $Ge_{23}Sb_{12}S_{65}$ glass

| A | $B_1$ | $B_2$ | $B_3$ | $C_1$ | $C_2$ | $C_3$ |
|---|---|---|---|---|---|---|
| 1 | 0.0415 | 0.0722 | 4.0043 | $0.0968\times10^{-12}$ | $174.0509\times10^{-12}$ | $0.0558\times10^{-12}$ |

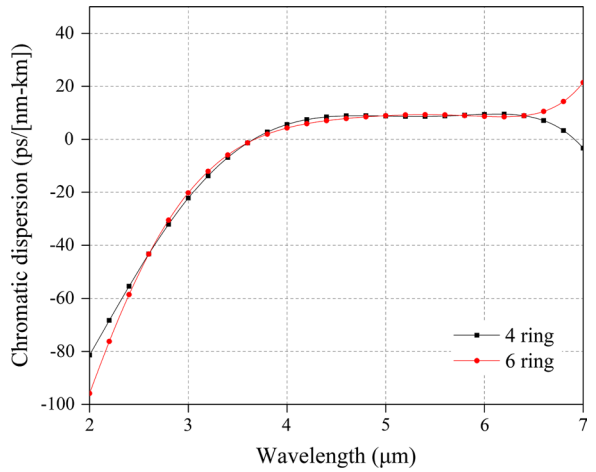


**Fig. 4** Chromatic dispersion curve of the optimized four-ring and six-ring ChG-PCFs

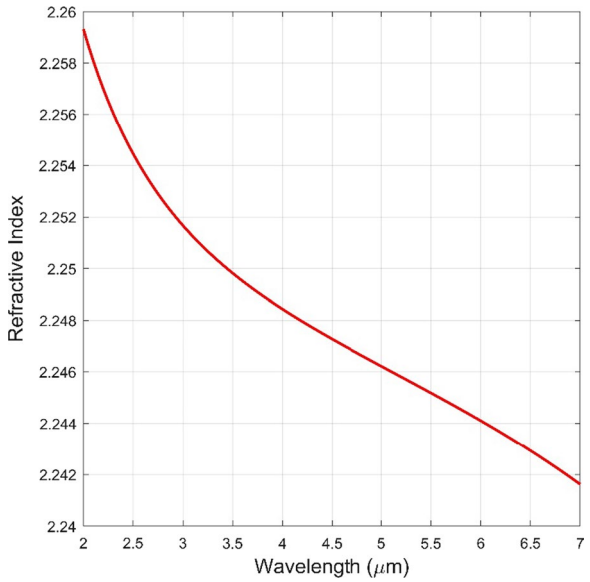


**Fig. 5** Plot of the material refractive index, $n_{eff}$ as a function of the wavelength

is a PCF structure with $\Lambda = 5$ μm, $d_1 = 1.4$ μm, $d_2 = 1.6$ μm, and a ZDW = 3.6 μm.

## 3 Results

The chromatic dispersion curve of the optimized $Ge_{23}Sb_{12}S_{65}$ based four-ring and six-ring chalcogenide PCF is plotted as a function of wavelength from 2 $\mu m$ to 7 $\mu m$ and is shown in Fig. 4. In the four-ring structure, the air holes in layers 1–3 are 1.4 $\mu$m in diameter, while the air holes in layer 4 are 1.6 $\mu$m in diameter. In the six-ring structure, the air holes in layers 1–3 are 1.4 $\mu$m in diameter, while the air holes in layers 4–6 are 1.6 $\mu$m in diameter. Both the PCF structures have a hole spacing (pitch, $\Lambda$) of 5 $\mu$m. With this optimized air hole diameters and pitch, the PCF achieved broad and flat dispersion profiles.

## 4 Discussions

Waveguide and material dispersion combine to form chromatic dispersion, $D(\lambda)$. Figure 5 shows the plot of the material refractive index of the $Ge_{23}Sb_{12}S_{65}$ glass as a function of the wavelength. Chromatic dispersion is a significant and pressing parameter of PCF, and it plays a vital role in fiber optic communication systems because it limits the optical fiber's data transmission capability. The pulses at various wavelengths propagate at differing speeds within the fiber due to chromatic dispersion. Pulse broadening occurs as a result of this. The chromatic dispersion curve in PCF can be tailored to the conditions required for practical applications.

The chromatic dispersion is defined by $D(\lambda)$ as [46]:

$$D(\lambda) = -\frac{\lambda}{c}\frac{d^2 Re[n_{\text{eff}}]}{d\lambda^2} \tag{2}$$

where $Re[n_{\text{eff}}]$ is the real part of the effective index obtained by computing the fundamental mode using the finite element method, $\lambda$ is the wavelength in micrometers, and c is the velocity of light in vacuum.

The effective index of the fundamental mode of $Ge_{23}Sb_{12}S_{65}$ based chalcogenide PCF fiber is calculated at the wavelength of interest using finite element method and the simulated result showed that the designed PCF was endlessly single mode. The calculated effective index, $n_{eff}$ as a function of the wavelength for the optimized six-ring PCF is shown in Fig. 6. The chromatic dispersion, $D(\lambda)$ is then calculated using Eq. 2 and the calculated values are plotted for the wavelength of interest.

The electric field distribution of the fundamental mode is shown in Fig. 7. This is the electric field

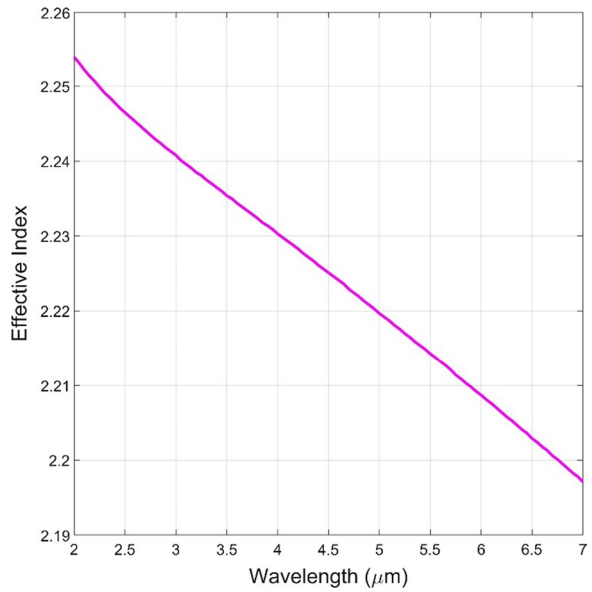


**Fig. 6** Plot of Effective index, $n_{eff}$ as a function of the wavelength for the optimized six-ring PCF

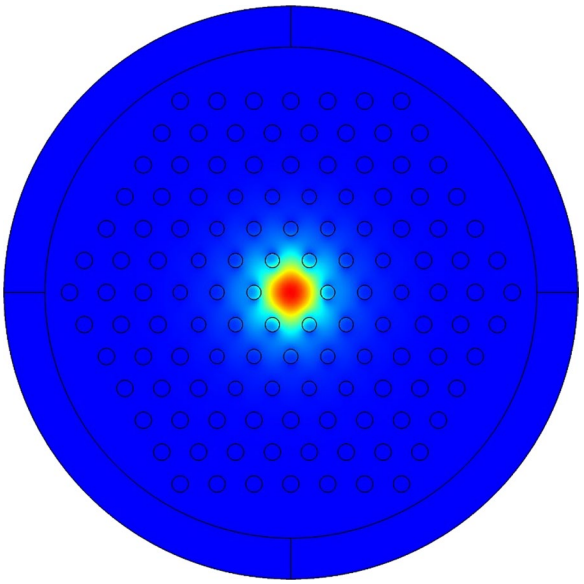

**Fig. 7** Electric field distribution of the fundamental mode in $Ge_{23}Sb_{12}S_{65}$ based chalcogenide PCF

distribution of the proposed six-ring PCF for the excitation wavelength 3 $\mu$m. Here in our proposed design, the core is of a high refractive index $Ge_{23}Sb_{12}S_{65}$ based chalcogenide glass, while the air holes act as cladding. No matter the wavelength, there is an intense light confinement inside the core due to the huge index difference between the core and cladding.

The second order dispersion coefficient ($\beta_2$) is defined by [46]

$$\beta_2 = -\frac{\lambda^2 D(\lambda)}{2\pi c} \tag{3}$$

Using Eq. 3, the $\beta_2$ values are calculated for the wavelength range of interest and then the $\beta_2$ graph is plotted as a function of wavelength. The data were then fitted with a curve, and the resulting polynomial was extracted. The Taylor series expansion of beta to the eighth term is given by [46]:

$$\beta_2(\omega) = \beta_2 + \beta_3\omega_R + \beta_4\frac{{\omega_R}^2}{2!} + \beta_5\frac{{\omega_R}^3}{3!} + \beta_6\frac{{\omega_R}^4}{4!} + \beta_7\frac{{\omega_R}^5}{5!} + \beta_8\frac{{\omega_R}^6}{6!} + \beta_9\frac{{\omega_R}^7}{7!} \tag{4}$$

The extracted polynomial from the $\beta_2$ curve is then matched to the Taylor series expansion given in Eq. 4 to get the higher order beta terms where,

$$\omega_R = \omega - \omega_o \ and \ \omega_o = \frac{2\pi c}{\lambda_0}$$

and , $\lambda_0 = 3.3\mu m$ is the pump wavelength of the laser. The higher order beta coefficients extracted from Taylor series expansion are listed in Table 2.

Choosing a right numerical method for computation is very important as it can highly improve the accuracy of the results and the computation time can be greatly reduced as well [47]. The chromatic dispersion of the fundamental mode $HE_{11}$ of the novel engineered $Ge_{23}Sb_{12}S_{65}$ based chalcogenide PCF is calculated for different configurations using a complete vectorial finite element method (FEM) by increasing the pitch, $\Lambda$ from 3.2 to 5 μm and fixing the smaller and larger air hole diameters as $d_1$=1.4 μm and $d_2$=1.6 μm, respectively, within the wavelength range of 2 to 7 μm. We have studied both four-ring as well as six-ring configurations. We ran numerous simulations to see how different values of

**Table 2** Taylor series expansion of the propagation constant

| Coefficient | Value |
|---|---|
| $\beta_2$ | $50.969\ ps^2/km$ |
| $\beta_3$ | $0.863\ ps^3/km$ |
| $\beta_4$ | $-0.00227\ ps^4/km$ |
| $\beta_5$ | $-5.277\times10^{-5}\ ps^5/km$ |
| $\beta_6$ | $2.502\times10^{-6}\ ps^6/km$ |
| $\beta_7$ | $5.5305\times10^{-7}\ ps^7/km$ |
| $\beta_8$ | $-5.341\times10^{-9}\ ps^8/km$ |
| $\beta_9$ | $-8.112\times10^{-11}\ ps^9/km$ |

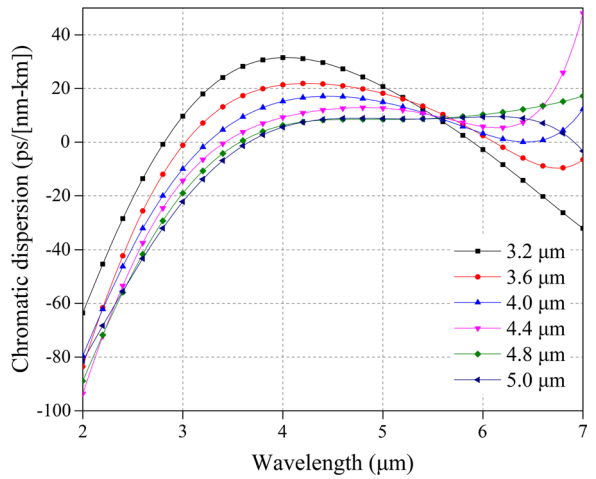


**Fig. 8** Chromatic dispersion of four-ring structure for variations in pitch from 3.2 to 5 μm

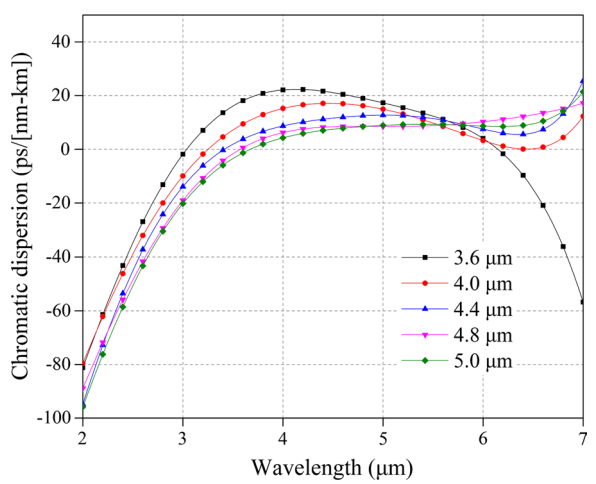


**Fig. 9** Chromatic dispersion of six-ring structure for variations in pitch from 3.6 to 5 μm

pitch affect dispersion characteristics. Figure 8 shows the chromatic dispersion curves in the increasing order of pitch for the four-ring PCF structure. Figure 9 shows the chromatic dispersion curves in the increasing order of pitch for the six-ring PCF structure. The plots are combined in same graph for both four-ring and six-ring configurations individually for a comparative study purpose. It can be clearly seen from Figs. 8 and 9 that as the pitch increases, the slope of the curve reduces resulting in an ultra-flat dispersion profile for the highest pitch value, 5 μm. Due to the combined effect of waveguide and material dispersion, the dispersion curve keeps getting flatter as the pitch was increased from 3.2 to 5 μm for both the four-ring and six-ring cases. It is also observed that the dispersion curves of the designed PCF remain in both normal and anomalous dispersion regime. It is a notable point that the zero-dispersion wavelength shifts to higher wavelengths when the pitch value is increased. The optimized geometrical parameters are $d_1 = 1.4$ μm, $d_2 = 1.6$ μm, and $\Lambda = 5$ μm. For the optimized geometrical parameters, the dispersion profile is flattened to within −3.41 to 9.5 ps/[nm–km] for the six-ring structure and −3.91 to 8.17 ps/[nm–km] for the four-ring structure in the wavelength range of 3500–6500 nm. The zero-dispersion wavelength (ZDW) for the optimized four-ring and six-ring PCF comes around 3.6 μm. At 3.3 μm, we learned that a PCF structure with $\Lambda = 5$ μm, $d_1 = 1.4$ μm, $d_2 = 1.6$ μm, and a ZDW = 3.6 μm is the most effective candidate for efficient SC generation.

## 5 Conclusion

The idea that a PCF's geometrically induced dispersion has extraordinary properties and that it is extremely tunable in terms of the fiber's geometrical parameters can be used to adjust the $Ge_{23}Sb_{12}S_{65}$ based chalcogenide glass material's intrinsic dispersion in various ways. As a whole, we were able to make a well-defined method for developing a broad range of dispersion behaviors in the mid-IR wavelength range. In this paper, we introduced a six-ring hexagonal chalcogenide PCF with broadband ultra-flattened MIR dispersion characteristics. Six layers of air holes, evenly spaced in a regular hexagonal pattern, made up the cladding. We could see how a clever use of the hexagonal photonic crystal fiber's geometry, allows for exceptional regulation of the fiber's dispersion properties. Greater engineering flexibility was made possible by purposely varying the spacing between two adjacent air holes (pitch). As the pitch was increased from 3.2 to 5 μm, the dispersion curve continued to flatten due to the combined effects of waveguide and material dispersion. For the proposed design, the air holes in layers 1–3 are fixed to 1.4 μm in diameter, whereas those in layers 4–6 are fixed to 1.6 μm in diameter. The PCF has air holes spaced 5 μm apart (pitch). In a broad wavelength range of 3.5 $\mu m$ to 6.5 $\mu$m, a flattened low dispersion between −3.41 and 9.5 ps/[nm–km] and −3.91 to 8.17 ps/[nm–km] was successfully achieved. It is also noteworthy that as the pitch value is raised, the zero-dispersion wavelength moves to higher wavelengths. The proposed chalcogenide PCF with nearly zero ultra-flattened dispersion properties can be employed for applications such as, soliton generation, gas sensing, biomedical imaging, supercontinuum generation, and long-distance high-speed communication applications in the mid-infrared wavelength region.

**Abbreviations**
MIR: Mid-Infrared; SC: Supercontinuum; PCF: Photonic crystal fiber; IR: Infrared; ChG: Chalcogenide; ZDW: Zero dispersion wavelength.

**Acknowledgements**
The authors would like to thank Melvin for the helpful discussions and Aruna for the technical support.

**Author contributions**
JRS carried out the fiber Supercontinuum studies, have done the coding to plot dispersion curves and drafted the manuscript. TJ carried out the studies on chalcogenide materials, and helped to draft the manuscript. CR participated in the design of the study. SPM performed the higher order dispersion analysis and participated in the design of the study. CR conceived of the study, and coordination and helped to draft the manuscript. All authors read and approved the final manuscript.

**Funding**
There is no funding available to carry out this research.

**Availability of data and materials**
The authors of the above titled paper hereby declare that the work included in the above paper is original and is an outcome of the research carried out by the authors indicated in it. All data generated or analysed during this study are included in this published article.

## Declarations

**Ethics approval and consent to participate**
Not applicable.

**Consent for publication**
Not applicable.

**Competing interest**
The authors declare that they have no competing interests. All co-authors have seen and agree with the contents of the manuscript and there is no financial interest to report.

**Author details**
[1]Department of Electronics and Communication Engineering, National Institute of Technology Calicut, Calicut, India. [2]Karunya Institute of Technology and Sciences, Department of Electronics and Communication Engineering, Karunya Nagar, Coimbatore, Tamil Nadu, India.

Received: 9 June 2022 Accepted: 3 August 2022
Published online: 19 August 2022

**References**

1. Dash JN, Jha R (2015) Fabry-Perot based strain insensitive photonic crystal fiber modal interferometer for inline sensing of refractive index and temperature. Appl Opt 54(35):10479–10486
2. Wadsworth W, Knight J, Reeves W, Russell P, Arriaga J (2000) Yb3+-doped photonic crystal fibre laser. Electron Lett 36:1452-1454(2). https://doi.org/10.1049/el_20000942
3. Taya SA, Doghmosh N, Abutailkh MA, Upadhyay A, Nassar ZM, Colak I (2021) Properties of band gap for p-polarized wave propagating in a binary superconductor-dielectric photonic crystal. Optik 243:167505. https://doi.org/10.1016/j.ijleo.2021.167505
4. Doghmosh N, Taya SA, Upadhyay A, Olaimat MM, Colak I (2021) Enhancement of optical visible wavelength region selective reflector for photovoltaic cell applications using a ternary photonic crystal. Optik 243:167491. https://doi.org/10.1016/j.ijleo.2021.167491
5. Taha TA, Mehaney A, Elsayed HA (2022) Detection of heavy metals using one-dimensional gyroidal photonic crystals for effective water treatment. Mater Chem Phys 285:126125. https://doi.org/10.1016/j.matchemphys.2022.126125
6. Segovia-Chaves F, Elsayed HA, Mehaney A (2021) Tunability in the terahertz range of a one-dimensional photonic quasicrystal containing an InSb semiconductor. Optik 245:167675. https://doi.org/10.1016/j.ijleo.2021.167675
7. Mehaney A, Abadla MM, Elsayed HA (2021) 1D porous silicon photonic crystals comprising Tamm/Fano resonance as high performing optical sensors. J Mol Liquids 322:114978. https://doi.org/10.1016/j.molliq.2020.114978
8. Abadla MM, Elsayed HA, Mehaney A (2020) Sensitivity enhancement of annular one dimensional photonic crystals temperature sensors with nematic liquid crystals. Phys Scr 95(8):085508. https://doi.org/10.1088/1402-4896/aba2b0
9. Ahmed AM, Elsayed HA, Mehaney A (2021) High-performance temperature sensor based on one-dimensional pyroelectric photonic crystals comprising tamm/fano resonances. Plasmonics 16(2):547–557. https://doi.org/10.1007/s11468-020-01314-4
10. Asaduzzaman S, Rehana H, Aziz MDT, Ahmed AM, Elsayed HA, Mehaney A (2022) Design of hexa-wheel sectored photonic crystal fiber for soybean biodiesel sensing. Phys Scr 97(3):030005. https://doi.org/10.1088/1402-4896/ac52cf
11. Elsayed HA, Taha TA, Algarni SA, Ahmed AM, Mehaney A (2022) Evolution of optical Tamm states in a 1D photonic crystal comprising a nanocomposite layer for optical filtering and reflecting purposes. Opt Quant Electron 54(5):312. https://doi.org/10.1007/s11082-022-03715-7
12. Møller U, Yu Y, Kubat I, Petersen CR, Gai X, Brilland L, Méchin D, Caillaud C, Troles J, Luther-Davies B, Bang O (2015) Multi-milliwatt mid-infrared supercontinuum generation in a suspended core chalcogenide fiber. Opt Expr 23:3282–3291
13. Schliesser A, Picqué N, Hänsch TW (2012) Mid-infrared frequency combs. Nat Photon 6(7):440–449. https://doi.org/10.1038/nphoton.2012.142
14. Eggleton BJ, Luther-Davies B, Richardson K (2011) Chalcogenide photonics. Nat Photon 5(3):141–148. https://doi.org/10.1038/nphoton.2011.309
15. Seddon AB (2011) A prospective for new mid-infrared medical endoscopy using chalcogenide glasses. Int J Appl Glass Sci 2(3):177–191. https://doi.org/10.1111/j.2041-1294.2011.00059.x
16. Ke K, Xia C, Islam MN, Welsh MJ, Freeman MJ (2009) Mid-infrared absorption spectroscopy and differential damage in vitro between lipids and proteins by an all-fiber-integrated supercontinuum laser. Opt Expr 17:12627–12640
17. Dupont S, Petersen C, Thøgersen J, Agger C, Bang O, Keiding SR (2012) IR microscopy utilizing intense supercontinuum light source. Opt Expr 20(5):4887–4892
18. Zhao Z, Wu B, Wang X, Pan Z, Liu Z, Zhang P, Shen X, Nie Q, Dai S, Wang R (2017) Mid-infrared supercontinuum covering 2.0–16 μm in a low-loss telluride single-mode fiber. Laser & Photon Rev 11(2):1700005. https://doi.org/10.1002/lpor.201700005
19. Izawa T, Shibata N, Takeda A (1977) Optical attenuation in pure and doped fused silica in the IR wavelength region. Appl Phys Lett 31(1):33–35. https://doi.org/10.1063/1.89468
20. Feng X, Shi J, Segura M, White NM, Kannan P, Loh WH, Calvez L, Zhang X, Brilland L (2013) Halo-tellurite glass fiber with low OH content for 2–5μm mid-infrared nonlinear applications. Opt Expr 21(16):18949–18954
21. Zhang Y, Kainerstorfer J, Knight JC, Omenetto FG (2017) Experimental measurement of supercontinuum coherence in highly nonlinear soft-glass photonic crystal fibers. Opt Expr 25(16):18842–18852
22. Calvez L (2017) Chalcogenide glasses and glass-ceramics: transparent materials in the infrared for dual applications. Comptes Rendus Physiq 18(5):314–322. https://doi.org/10.1016/j.crhy.2017.05.003
23. Tripathi S, Kumar B, and Dwivedi DK (2018) Chalcogenide glasses: thin film deposition techniques and applications in the field of electronics. In: 2018 5th IEEE Uttar Pradesh Section International Conference on Electrical, Electronics and Computer Engineering (UPCON), 2–4, pp 1–4, https://doi.org/10.1109/UPCON.2018.8597029
24. Wang J, Vogel E, Snitzer E (1994) Tellurite glass: a new candidate for fiber devices. Opt Mater 3(3):187–203
25. Ferrando A, Silvestre E, Miret J, Monsoriu J, Andrés M, Russell PS (1999) Designing a photonic crystal fibre with flattened chromatic dispersion. Electron Lett 35:325-327(2). https://doi.org/10.1049/el_19990189

26. Reeves W, Knight J, Russell P, Roberts P (2002) Demonstration of ultra-flattened dispersion in photonic crystal fibers. Opt Expr 10(14):609–613
27. Faisal M, Mia MB, Chowdhury KR, Ani AB, Ghosh S, and Naz SI (2018) Heptagonal photonic crystal fiber for dispersion compensation with a very low confinement loss. In: 2018 10th international conference on electrical and computer engineering (ICECE), pp 257–260
28. Fiaboe KF, Kumar P, Roy JS (2019) Flattened zero dispersion Photonic crystal fibers with embedded nano holes and ultra low confinement loss for supercontinuum generation. Adv Electromagn 8(4):7–15
29. Ani AB and Faisal M (2016) Ultra-flattened broadband dispersion compensating photonic crystal fiber with ultra-low confinement loss. In: 2016 9th international conference on electrical and computer engineering (ICECE), pp 243–246
30. Ferrando A, Silvestre E, Andres P, Miret JJ, Andres MV (2001) Designing the properties of dispersion-flattened photonic crystal fibers. Opt Expr 9(13):687–697
31. Namihira Y, Hossain MA, Liu J, Koga T, Kinjo T, Hirako Y, Begum F, Kaijage SF, Razzak SMA, and Nozaki S (2011) Dispersion flattened photonic crystal fibers for supercontinuum generation in a telecommunication window. In: IET international conference on communication technology and application (ICCTA 2011), pp 815–818
32. Klimczak M, Siwicki B, Skibi´nski P, Pysz D, Stepie´n R, Heidt A, Radzewicz C, Buczynski R (2014) Coherent supercontinuum generation up to 2.3 μm in all-solid soft-glass photonic crystal fibers with flat all-normal dispersion. Opt Expr 22(15):18824–18832
33. Liao J, Sun J, Du M, Qin Y (2014) Highly nonlinear dispersion- flattened slotted spiral photonic crystal fibers. IEEE Photon Technol Lett 26(4):380–383
34. Matsui T, Zhou J, Nakajima K, Sankawa I (2005) Dispersion-flattened photonic crystal fiber with large effective area and low confinement loss. J Lightw Technol 23(12):4178–4183
35. Singh S, Upadhyay A, Sharma D, Taya SA (2022) A comprehensive study of large negative dispersion and highly nonlinear perforated core PCF: theoretical insight. Phys Scr 97(6):065504. https://doi.org/10.1088/1402-4896/ac6d1a
36. Upadhyay A, Singh S, Sharma D, Taya SA (2021) Analysis of proposed PCF with square air hole for revolutionary high birefringence and nonlinearity. Photon Nanostruct - Fundam Appl 43:100896. https://doi.org/10.1016/j.photonics.2021.100896
37. Upadhyay A, Singh S, Sharma D, Taya SA (2021) A highly birefringent bend-insensitive porous core PCF for endlessly single-mode operation in THz regime: an analysis with core porosity. Appl Nanosci 11(3):1021–1030. https://doi.org/10.1007/s13204-020-01664-9
38. Upadhyay A, Singh S, Sharma D, Taya SA (2021) An ultra-high birefringent and nonlinear decahedron photonic crystal fiber employing molybdenum disulphide (MoS2): a numerical analysis. Mater Sci Eng B 270:115236. https://doi.org/10.1016/j.mseb.2021.115236
39. Pleitez MA, Hertzberg O, Bauer A, Seeger M, Lieblein T, Lilienfeld-Toal HV, Mantele W (2015) Photothermal deflectometry enhanced by total internal reflection enables non-invasive glucose monitoring in human epidermis. Analyst 140:483–488. https://doi.org/10.1039/C4AN01185F
40. Nguyen M-H, Tsai H-J, Wu J-K, Wu Y-S, Lee M-C, Tseng F-G (2013) Cascaded nano-porous silicon for high sensitive biosensing and functional group distinguishing by Mid-IR spectra. Biosens Bioelectron 47:80–85
41. Kalantari M, Karimkhani A, Saghaei H (2018) Ultra-Wide mid-IR supercontinuum generation in As2S3 photonic crystal fiber by rods filling technique. Optik 158:142–151. https://doi.org/10.1016/j.ijleo.2017.12.014
42. Shen LP, Huang WP, Chen GX, Jian SS (2003) Design and optimization of photonic crystal fibers for broad-band dispersion compensation. IEEE Photon Technol Lett 15(4):540–542. https://doi.org/10.1109/LPT.2003.809322
43. Hansen KP, Folkenberg JR, Peucheret C, and Bjarklev A (2003) Fully dispersion controlled triangular-core nonlinear photonic crystal fiber.In: OFC 2003 optical fiber communications conference, 28–28, pp. PD2–1, https://doi.org/10.1109/OFC.2003.316021
44. Tzong-Lin W, Chia-Hsin C (2005) A novel ultraflattened dispersion photonic crystal fiber. IEEE Photon Technol Lett 17(1):67–69. https://doi.org/10.1109/LPT.2004.837475
45. Poli F, Cucinotta A, Selleri S, Bouk AH (2004) Tailoring of flattened dispersion in highly nonlinear photonic crystal fibers. IEEE Photon Technol Lett 16(4):1065–1067. https://doi.org/10.1109/LPT.2004.824624
46. Agrawal G (2012) Nonlinear fiber optics, 5th ed. Elsevier Academic Press
47. Raja SJ, Rao SS, Charlcedony R (2020) Design and analysis of dispersion-compensating chalcogenide photonic crystal fiber with high birefringence. SN Appl Sci 2(3):499. https://doi.org/10.1007/s42452-020-2308-0


## Publisher's Note